Electronic Supplementary Material (ESI) for Materials Chemistry Frontiers.

Exploiting synergistic effect of multiphase MnO_2 stabilized by integrated conducting network for aqueous zinc-ion batteries

Na Fu [a], Qingyuan Zhao [a], Yuting Xu [a], Hongrui Wang [a], Junping Hu [a], Yuping Wu[c], Linlin Yang[d*], Xiongwei Wu [a,b*], and Xianxiang Zeng [a*]

[a] School of Chemistry and Materials Science, Hunan Agricultural University, Changsha, Hunan 410128, P. R. China

[b] School of Electrical and Information Engineering, Hunan University, Changsha, Hunan 410082, P.R. China

[c] School of Energy and Environment, Southeast University, Nanjing, Jiangsu, 210018, P.R. China

[d] Shanghai Electric Lingchu Energy Storage Technology Co., Ltd, Shanghai, 201800, P.R. China

Corresponding authors.

*E-mail addresses: yanglinlinzh@163.com (Lin-Lin Yang); wxwcsu05@aliyun.com (Xiong-Wei Wu); xxzeng@hunau.edu.cn (Xian-Xiang Zeng)

Experimental Section

Preparation of δ-MnO_2 Electrode: The δ-MnO_2 was synthesized by simply

heated the $KMnO_4$ precursor at 800℃ for 5h in the muffle furnace. The resulting brown powder product was collected by filtration, washed by Distilled Deionized water and left to dry in ambient condition overnight.

Preparation of α-MnO_2 Electrode: The α-MnO_2 nanorods were synthesized based on procedure in literature with slight modifications.[1] 15mL of 0.2 mol / L $KMnO_4$ and 15mL 0.6 mol / L $MnSO_4 \cdot H_2O$ were first mixed and stirred at 400 rpm for 2 h, transferred into a 50 mL Teflon-line stainless steel autoclave, and reacted at 150℃ for 8h. after cooling down to room temperature, the precipitate was collected by filtration, washed by Distilled Deionized water and ethanol for several times. Lastly, the products were dried at 80℃ for 12 h.

Preparation of CMO Electrode: The 3D material was synthesized by first mixing α-MnO_2 and δ-MnO_2 with a 1:2 weight ration. Then, The CMO slurry was prepared by mixing 3D material, super P carbon and polyvinylidene fluoride with a 7:2:1 weight ration in N-Methyl-2-pyrrolidene. The slurry was doctor bladed onto a carbon paper and left to dry in an over at 80℃ overnight. The active material loading of the electrode is ~2 mg cm^{-1}.

Preparation of CMOP Electrode: The PEDOT layer was then coated on the surface of CMO by electrodeposition in a solution of 0.008 mol L^{-1} 3,4-ethylenedioxythiophene, 0.01 mol L^{-1} lithium perchlorate, and 0.014 mol L^{-1} sodium dodecyl sulfate at 1.0 V for 300s at room temperature.

Electrochemical Measurement: The PEDOT electrodeposition processes was achieved by a CHI760D workstation and traditional three electrode cell using a Pt

wire as counter electrode, an Ag / AgCl as reference electrode and a 10*10 mm carbon cloth as working electrode in room temperature. Cyclic voltammetry, galvanostatic charge / discharge measurements, and electrochemical impedance spectroscopy were conducted employing a CHI760D workstation. The electrochemical characterizations of the aqueous battery were performed in a solution of 2 mol L^{-1} $ZnSO_4$ and 0.1 mol L^{-1} $MnSO_4$.

Material Characterization: The microstructures and compositions of the electrode materials were analyzed using filed-emission SEM (JEOS-6701F), TEM (HT7700), Raman spectroscopy (LabRAM HR Evolution)，XPS (Thermo Kalpha, Thermo ESCALAB 250XI), and XRD (XRD-6000)，FTIR (ALPHR).

Computational Methods: Density functional theory calculations were conducted in the Vienna Ab-initio Simulation Package (VASP) with which the projector augmented wave (PAW) formalism was implemented.[2-4] The energy cutoff is 450 eV and the calculations of energy and force were set to 10^{-5} eV and 0.05 eV $Å^{-1}$ per atom. The k-point mesh of the Brillouin zone was sampled to a 5×5×1 grid for structure optimizations.[5] The adsorption energies (Ea) formula was Ea =EZn+ Esubstrate - E(Zn-substrate), where EZn, Esubstrate, and E(Zn-substrate) represent the total energy of the Zn, different substrate surfaces, and the energy of the Zn adsorption on the different substrates.

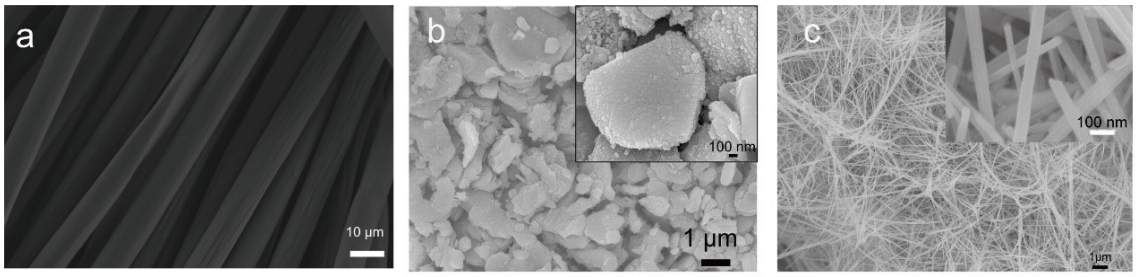

Fig. S1. a) SEM image of a carbon cloth substrate. b) Low-and high-(inset) magnification SEM image of α-MnO_2 and c) δ-MnO_2.

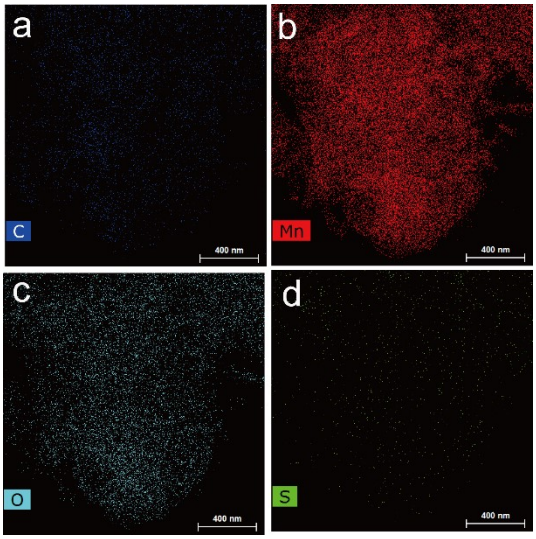

Fig. S2. Mappings for elements of a) C; b) Mn; c) O; d) S for DMOP cathode material.

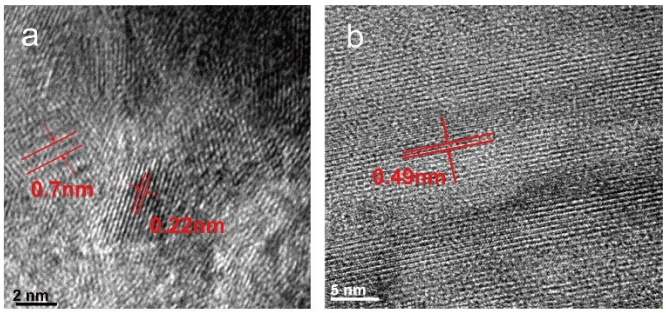

Fig. S3. a) TEM image of δ-MnO_2 and α-MnO_2.

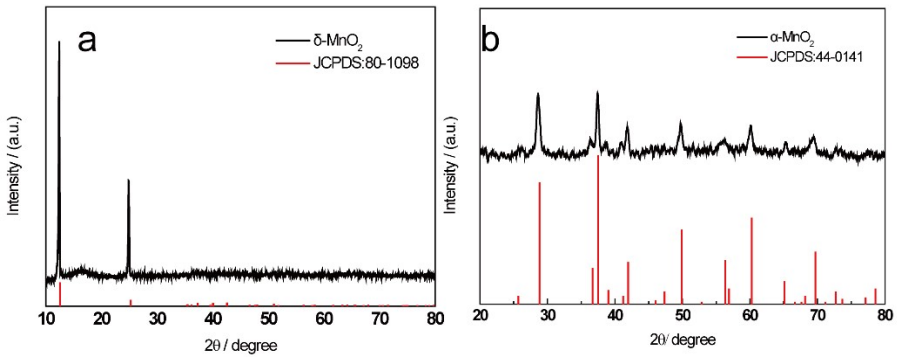

Fig. S4. a) XRD image of δ-MnO_2 and α-MnO_2.

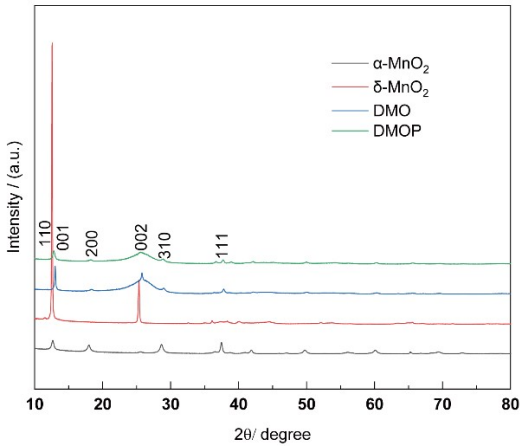

Fig. S5. XRD image comparison of different electrode materials.

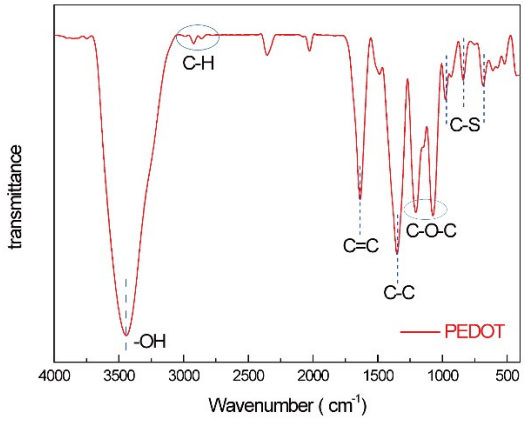

Fig. S6. FTIR spectra of pure poly (3,4-ethylenedioxythiophene) (PEDOT).

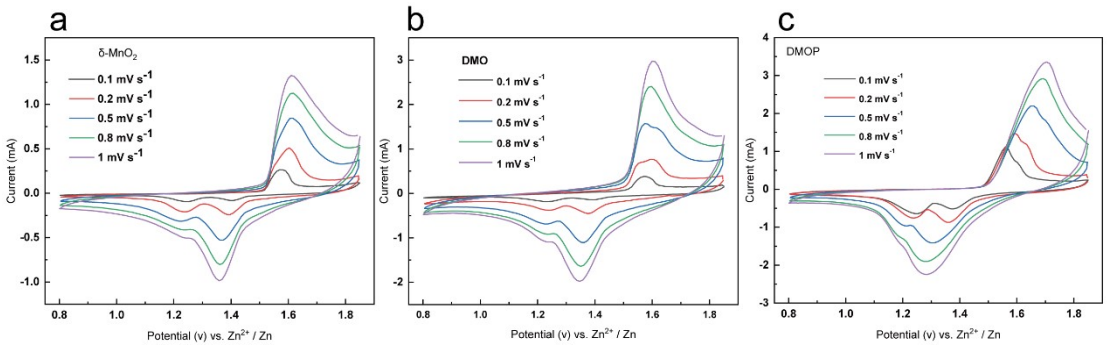

Fig. S7. CV curves collected at different scan rates of a) δ-MnO_2, b) DMO and c) DMOP.

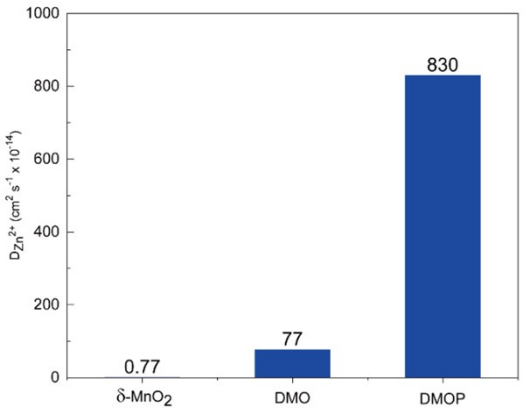

Fig. S8. Comparison of the ion diffusion coefficient of δ-MnO_2, DMO and DMOP electrodes.

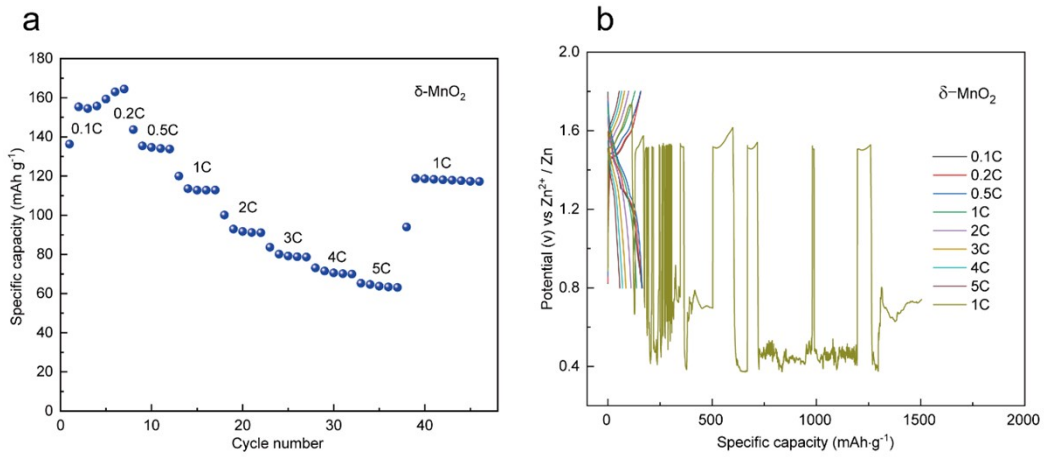

Fig. S9. a and b) Charge-discharge curves of δ-MnO_2 at the indicated current density.

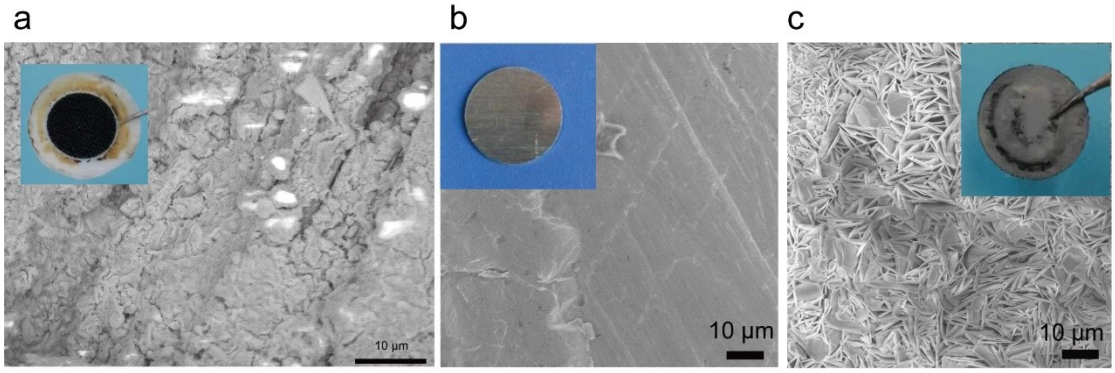

Fig. S10. a) SEM image after electrochemical reaction of δ-MnO_2 cathode material. b) pure Zn anode, c) Zn anode after electrochemical reaction of δ-MnO_2 cathode material.

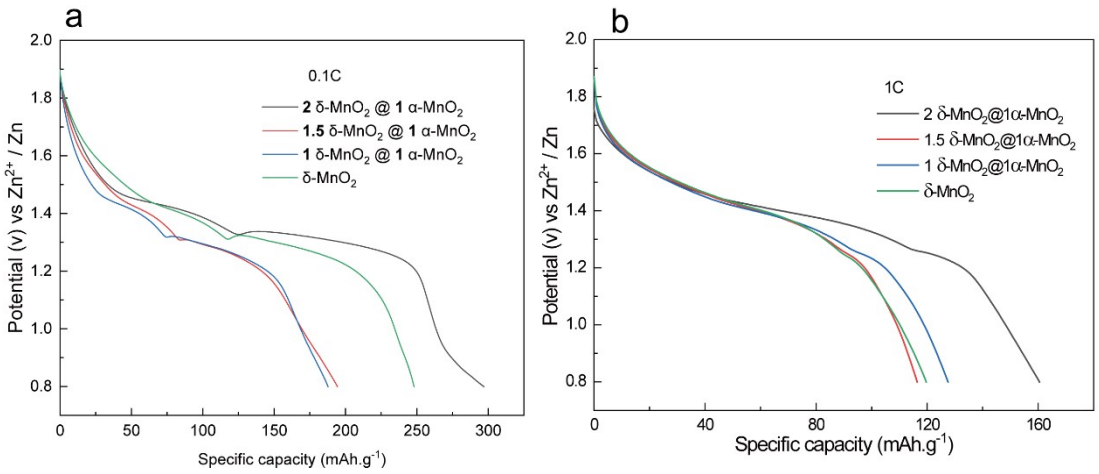

Fig. S11. Discharge curves of α-MnO_2 and δ-MnO_2 composites with different mass ratios a) at the first cycle. b) at 1C.

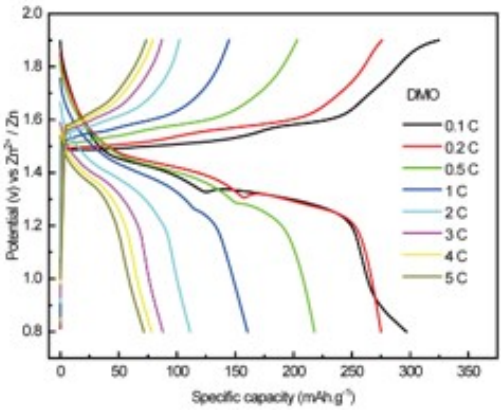

Fig. S12. a) Charge-discharge curves of DMO electrode at the indicated current density.

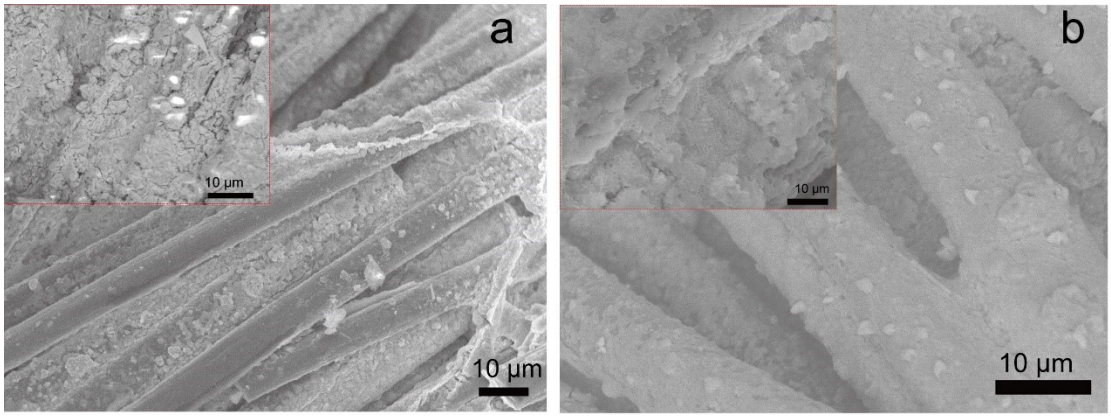

Fig. S13. a) SEM image after electrochemical reaction of δ-MnO_2 cathode material; b) SEM image after electrochemical reaction of DMO cathode material.

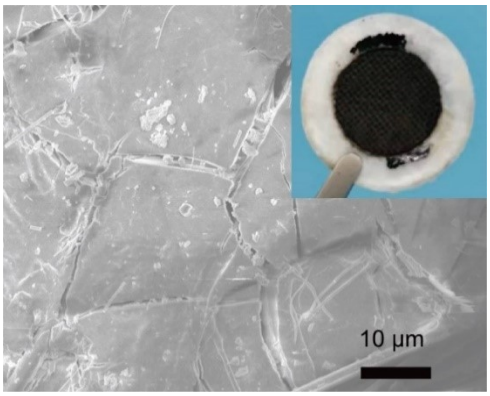

Fig. S14. SEM image after electrochemical reaction of DMOP cathode material.

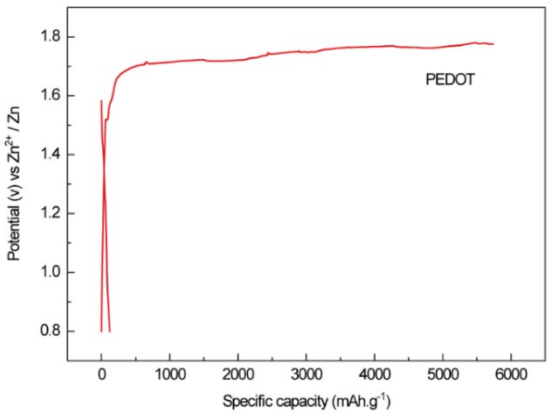

Fig. S15. Charge-discharge curves of pure PEDOT electrode at various current density.

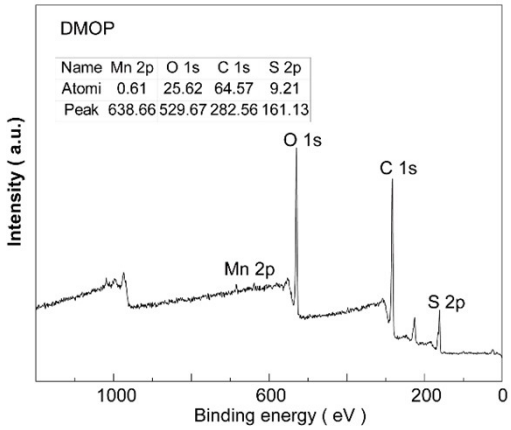

Fig. S16. X-ray photoelectron spectroscopy (XPS) of DMOP under stepwise Ar^+ sputtering.

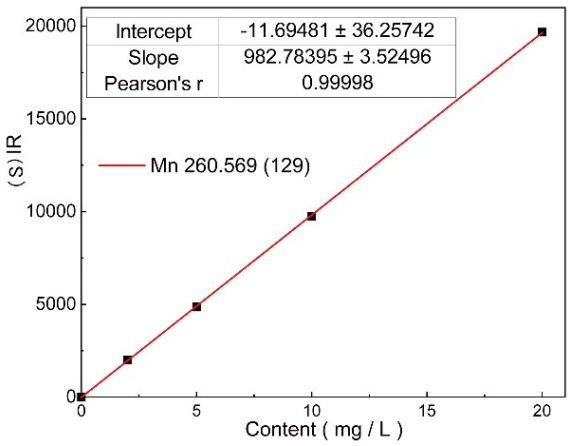

Fig. S17. Mn element standard curve of ICP test

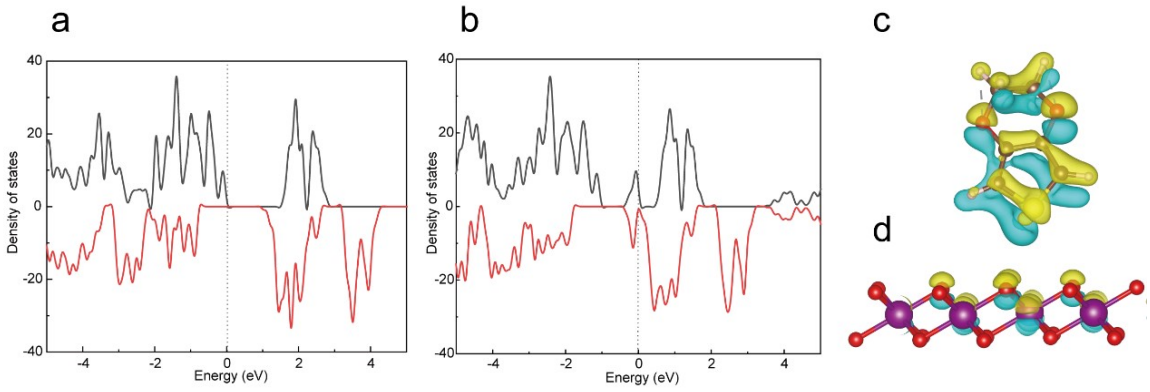

Fig. S18. a) Total density of states for MnO_2 and b) MnO_2-PEDOT. The Fermi level is set to be zero. c) Differential charge density in MnO_2 and d) PEDOT.

References

(1) Guo, Y.; Li, L.; Song, L.; Wu, M.; Gao, Y.; Chen, J.; Mao, C.; Song, J.; Niu, H. Co^{2+} induced phase transformation from δ- to α-MnO_2 and their hierarchical α-MnO_2@δ-MnO_2 nanostructures for efficient asymmetric supercapacitors. *J. Mater. Chem. A* **2019**, *7* (20), 12661-12668, DOI: 10.1039/c9ta01918a.

(2) Hohenberg, P.; Kohn, W. Inhomogeneous Electron Gas. *Phys. Rev.* **1964**, *136* (3B), B864-B871, DOI: 10.1103/PhysRev.136.B864.

(3) G. Kresse av, J. Furthmiiller. Efficiency of ab-initio total energy calculations for metals and semiconductors using a plane-wave basis set. *Phys. Rev. B* **1996**, *54*, 11169, DOI: 10.1016/0927-0256(96)00008-0.

(4) G. Kresse, J. Furthmu¨ller. Efficient iterative schemes for ab initio total-energy

calculations using a plane-wave basis set. *Comput. Mater. Sci.* **1996**, *6*, 15, DOI: 10.1103/physrevb.54.11169.

(5) Zhang, F.; Guo, X.; Xiong, P.; Zhang, J.; Song, J.; Yan, K.; Gao, X.; Liu, H.; Wang, G. Interface Engineering of MXene Composite Separator for High-Performance Li–Se and Na–Se Batteries. *Adv. Energy Mater.* **2020**, *10*(20), DOI: 10.1002/aenm.202000446